



INFLUENCE OF THE ROTATION SPEED ONTO COMPACT AXIAL FANS BROADBAND NOISE AT CONSTANT DESIGN POINT

Julien GRILLIAT ¹, Patrick BUCHWALD ³, Wolfgang LAUFER ¹,
Andreas LUCIUS ², Marc SCHNEIDER ², Damian VOGT ³,
Michael B. SCHMITZ ⁴

¹ *ebm-papst St. Georgen GmbH & Co.KG, Hermann-Papst-Straße 1,
78112 St. Georgen, Germany*

² *ebm-papst Mulfingen GmbH & Co. KG, Bachmühle
274673 Mulfingen, Germany*

³ *Institute of Thermal Turbomachinery and Machinery Laboratory (ITSM),
University of Stuttgart, Pfaffenwaldring 6, 70569 Stuttgart, Germany*

⁴ *Siemens AG, Zug, Switzerland.*

SUMMARY

The present paper investigates the problem of finding the optimal design rotation speed when both operating point and fan diameter are given. Under such constraints, rotational speed and blade loading are tightly connected. Validation measurements to a previously published CAA study are presented in detail and a sufficient agreement with the simulations is found. The measurements are finally post-processed so that the broadband contribution is highlighted. An optimal rotation speed is found which minimizes the broadband contribution.

INTRODUCTION

In most industrial projects, operating point and design volume flow rate are given, which means that very little freedom is let to adjust the fan diameter. Once these variables are set, the fan rotation speed remains the only variable the fan developer can freely choose. Usual design rule tend to reduce the rotation speed at its minimum, since most of aeroacoustic phenomena scale with the blade tip velocity. Though, recent studies [1,2] showed that this strategy has limited potential. The lower the rotation speed, the higher the blade has to be loaded in order to reach the operating point. Blade loading is highly correlated with broadband noise, as the blade boundary layers are thickened

and tip leakage flow strengthened. At the worst case, the flow might even detach from the blade, leading to drastic noise increase. The hypothesis of an optimal rotation speed can thus be formulated. This idea is illustrated on the Figure 1.

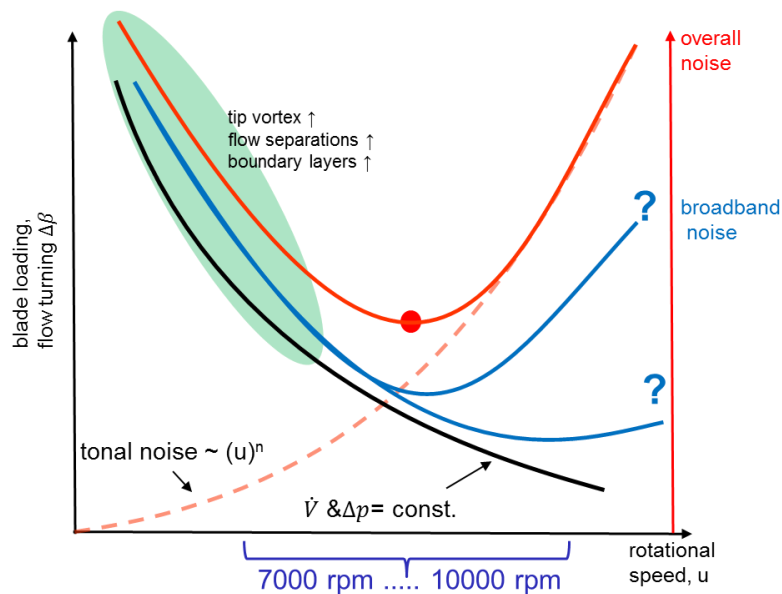


Figure 1: Influence of the rotation speed onto fan noise.

In order to investigate this idea, an operating point (800 m³/h, 400 Pa) has been selected, and five different rotation speeds covering a range from 7000 to 10000 rpm have been chosen. The same blade loading has been used for all fans, and the fan depth has been adapted. A thorough numerical study has been carried out and previously published by Buchwald & al [3].

The present communication aims at showing the validation measurements following the CFD study and highlighting some relationships between fan rotation speed and broadband noise. The study is organized as follows. The challenges met during prototype realization are presented in a first part, along with the measurement facility. In a second part, measurements are compared to the results of the aforementioned CFD analysis. A third part is devoted to the further analysis of tonal/broadband noise ratio depending on the rotation speed. All results are summarized in the conclusion.

PROTOTYPE REALIZATION AND MEASUREMENT

The validation study was carried out at ebm-papst Sankt Georgen in parallel to development activities, and therefore had to cope with the same constraints as any industrial development project: delays, costs and manpower. This led the project to choose the following main concept: rotors and pieces from the casing are realized with help of rapid prototyping and assembled on a carrying structure. This structure is composed of a plate, the struts and a casing. Rotor and motor are mounted on the plate, whereas inflow and outflow nozzles are mounted on the structure casing. This casing is also used to mount the prototype to the wind tunnel test section. This concept presents advantages and drawback. On one hand, 3D-printed parts are much cheaper than milled from aluminium. Furthermore, the same motor, driving electronic and structure can be reused for each prototype. On the other hand, each prototype has to be destroyed so that the next one can be mounted.

A comparison between the numerical model and its practical realization is presented on the Figure 2. Since the targeted rotation speeds are quite high, minor deviations from the original geometry were carried out. Balancing pockets were designed on the rotor hub in order to prevent imbalance from influencing the acoustic measurements. This led to slight discrepancies in the hub

inlet region. Moreover, the struts geometry was changed from 2 mm diameter cylinders to ellipses with a 4 mm axis in the longitudinal direction, so that the carrying structure withstands the rotor dynamics. Finally, power wires were mounted externally and fixed to a strut, since a concept with wires mounted through hollow struts would have been mechanically too weak.

The tip clearance has been measured for all prototypes, since this parameter plays a tremendous role for fan noise. These measurements have been carried out at five different positions depicted on the Figure 2 (bottom right), for each blade. The results are summarized in the Table 1. The averaged tip clearance is 1.38 mm, which corresponds to 38 % oversize with respect to the CFD. Moreover, a greater leakage is measured at positions 1 and 5 than at position 3, which shows that the casing is not perfectly round.

As the numerical models include very thin blades, the 3D-printed rotors were reinforced with resin infiltration. As a result, the rotors are mechanically stiffer and the expected deformation under rotation should be reduced.

Table 1: Fan tip clearance in mm.

Design rotation speed	Position 1	Position 2	Position 3	Position 4	Position 5	CFD
7000 rpm	1.5 – 1.6	1.3 – 1.4	1.0 – 1.1	1.1 – 1.2	1.4 – 1.5	1.0
7500 rpm	1.7 – 1.9	1.3 – 1.5	1.1 – 1.3	1.2 – 1.4	1.6 – 1.8	1.0
8000 rpm	1.5 – 1.6	1.3 – 1.4	1.0 – 1.1	1.1 – 1.2	1.5 – 1.6	1.0
9000 rpm	1.5 – 1.6	1.3 – 1.4	1.0 – 1.1	1.1 – 1.2	1.4 – 1.5	1.0
10000 rpm	1.7	1.5 - 1.6	1.1 – 1.2	1.2 – 1.3	1.7 – 1.8	1.0

In addition to this, a second concept (hereafter called alternative mock-up) in which the carrying structure has been removed has been used for moment measurements. The aggregate rotor/motor has thereby been directly mounted on a reaction moment test rig.



Figure 2: Comparison between numerical model (left) and prototype (right)

The measurements were carried out at the anechoic wind tunnel from ebm-papst Sankt Georgen, which consists of a closed-loop wind tunnel with suction and pressure side rooms dimensions of respectively $3.3 \times 3.05 \times 6.35 \text{ m}^3$ and $6.3 \times 4.5 \times 10.75 \text{ m}^3$. The sound power is computed according to ISO 3746: the microphone SPL are not corrected according to the distance from the prototype and are directly averaged. Every microphone signal is recorded 30 seconds at a 65 536 Hz sampling frequency. The narrow band spectra were computed with 1 Hz resolution and observed up to 20 000 Hz

For safety reasons, each prototype has first been measured at reduced speed. The rotation speed has been increased stepwise and a characteristic field has been investigated. In order to reach the design point, an extra characteristic has been measured at enhanced rotation speed if needed.

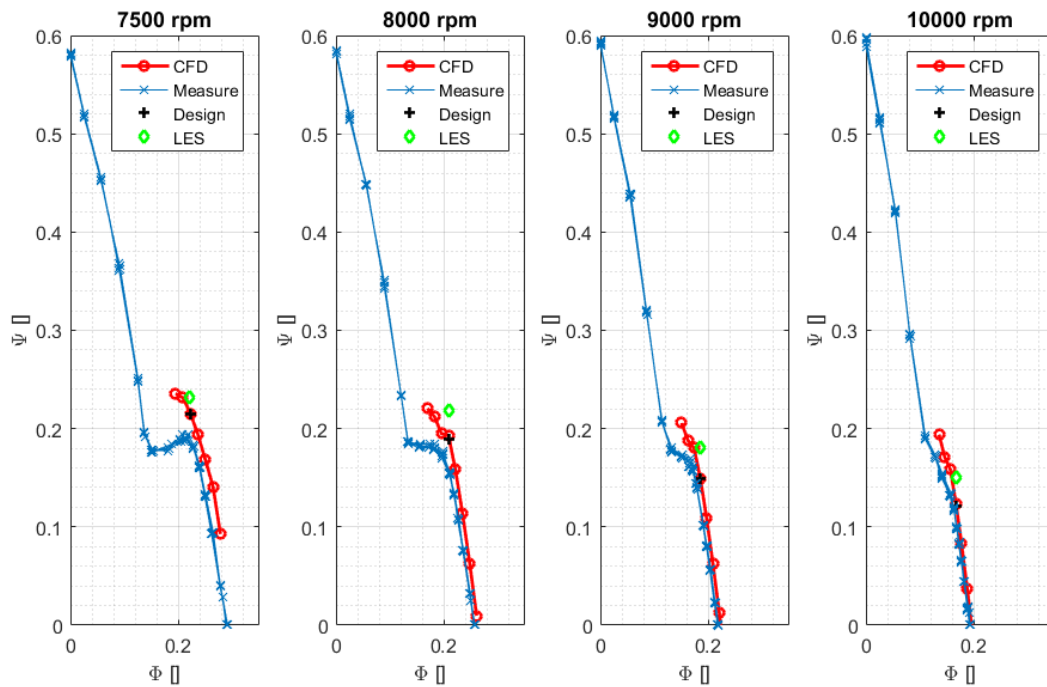


Figure 4: Hydraulic characteristic overview. Measurements at different speeds (blue) and RANS predictions (red). Design point and LES results are respectively represented in black and green

COMPARISON WITH CFD/CAA

An overview of the hydraulic characteristics is given on Figure 4. In order to compare measurements at different rotation speeds, a representation in the Φ - Ψ domain (flow coefficient, pressure coefficient) has been chosen. For each prototype, all measurements curves lie over each other, which shows that the centrifugal forces caused deformations have been very little and most probably did not influence the results. Interestingly, the greater the design rotation speed, the better the curves lie over each other.

The RANS based CFD predictions overpredicted the fan performances, which is a result one could expect with the present numeric set-up (RANS, periodic sector model with mixing plane). Interestingly, CFD & measure based characteristics exhibit the same behavior up to the saddle point. The best fit between CFD and measurements is obtained for the greatest design rotation speed. It is thus suspected that the greater tip clearances in the measurement do play a significant role. As the design rotation speed is decreased, the blade loading and therefore the tip leakage losses are increased, which is coherent with the greater discrepancies. As a consequence, the operating rotation speed has to be enhanced in order to reach the design point (s. Fig. 5 for the 9000 rpm fan). The table 2 shows the required rotation speed for all fans. For the 7000 rpm design fan, the

operating point lies in the unstable operating range and the operating point was not reached despite of an increase in rotation speed to 7500 rpm.

Table 2: Fan rotation speeds at design point.

Design rotation speed	7000 rpm	7500 rpm	8000 rpm	9000 rpm	10000 rpm
Rotation speed at design point	Failed	8000 rpm	8500 rpm	9400 rpm	10000 rpm

A LES simulation has been carried out on the basis of the RANS results at the design points. The switch from RANS to LES resulted in an increase of the pressure rise, and therefore enhanced the disparities between measurements and simulation.

The acoustic results will be illustrated with the 9000 rpm design prototype. An overview of the hydraulic characteristic field can be found on Figure 5. The corresponding sound power characteristic field is depicted on Figure 6. An extra characteristic has been measured at 9400 rpm in order to reach the design point. Moment measurements were carried out with the alternative mock-up, and moment characteristic as well as efficiency can be found on Figure 7. As the alternative mock-up does not include struts, the fan performances are a bit overestimated. As a consequence, only 9300 rpm were required to draw a characteristic reaching the design point.

The measured and RANS simulated rotor total efficiencies are reported in the Table 3 for the design point. Maximal rotor total efficiencies are reported too. As expected, the measured efficiencies lie over the simulated one, which is due to the slightly modified mock-up. Though, the same trend can be observed: as the design speed rises, the maximal achievable efficiency rises too. Besides, the measurements exhibit another interesting phenomenon: as the design rotation speed rises, the difference between efficiency at design point and maximal efficiency increases. This is due to the fact that the maximal efficiency is observed at decreasing flow rates.

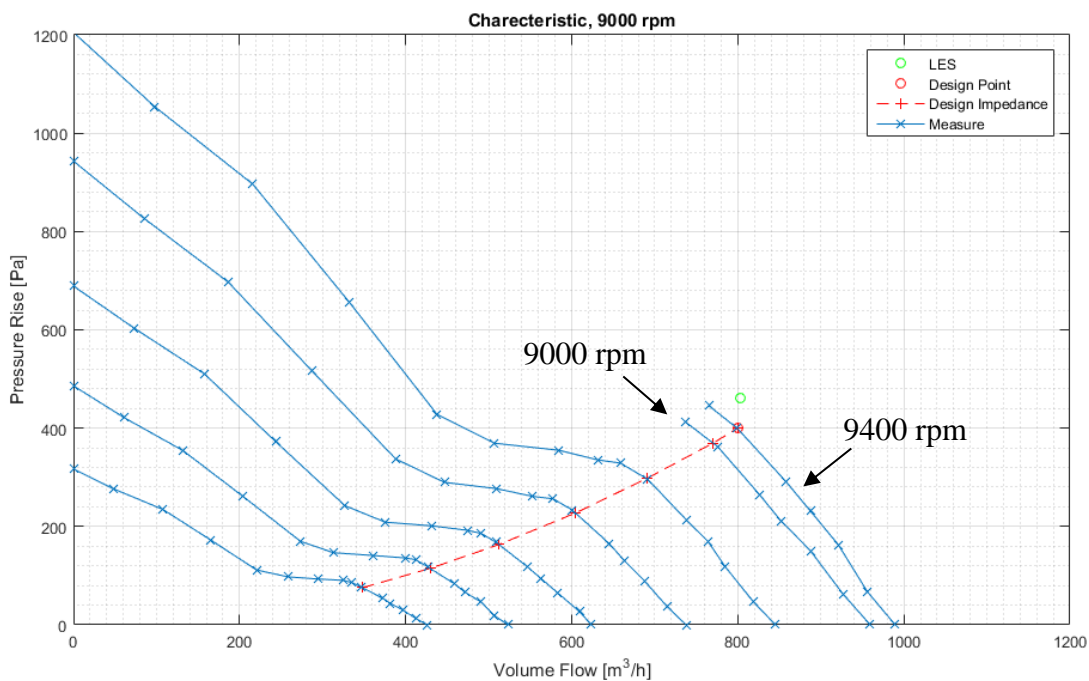


Figure 5: Hydraulic characteristic of the 9000 rpm design prototype. Measurements at different speeds (blue) and along the design impedance (dashed red)). Design point and LES results are respectively represented with red and green circles.

Table 3: fan rotor total efficiency

Design rotation speed	Efficiency at design point		Maximum efficiency	
	Measure	RANS	Measure	RANS
8000 rpm	44 %	49 %	52 %	49 %
9000 rpm	48 %	49 %	53 %	51 %
10000 rpm	52 %	47 %	54 %	52 %

Attempts to normalize the SWL characteristics are presented on the Figure 7 (right). It has been observed for all fans that the SWL curves overlap quite fairly in the unstable region (partial load operating range) for a normalization in 5.5^{th} power of the rotation velocity, whereas a 5^{th} power normalization gives reasonable results in the stable region (overload operating range). This is illustrated for the suction side (s. Fig. 7 top right) and pressure side (s. Fig. 7 bottom right) respectively. As the stable region is the most interesting one, all SWL curves (both pressure and suction side) will be normalized in the following with the 5^{th} power of the rotation speed. For each fan, the reference rotation speed used to build the normalized SWL (hereafter called SWLeq) will be the respective design rotation speed.

In order to compare measurements with simulation as done on Figure 8, the microphone recordings were not A-weighted, and a narrow-band PSD (1 Hz resolution) has been computed an integrated between 100 Hz and 4000 Hz. Surprising phenomena can be observed on the Figure 6 as well as on the characteristic field from the other prototypes. First, the characteristics present no real best acoustic point. Indeed, the quietest point is reached in free flow conditions, whereas most fans are louder at this point than at in their best efficiency point neighborhood. Though, the transition to partial load is clearly visible, as all characteristics present a drastic SWL increase. Moreover, points along the same impedance in the overload domain exhibit abnormal noise. This phenomenon is investigated in the following section. Finally, the design impedance lies in the lower range of the best efficiency domain, and there left from the local best acoustic impedance. A further examination results showed that the design impedance is closest to the local minimum for the 9000 rpm case.

Figure 5 and 6 explain why a direct comparison between predications and measurements is difficult. As mentioned earlier, the switch from RANS to LES resulted in an increase of the pressure rise, which shifted the operating point away from design toward higher impedances. A fair comparison therefore requires that the results are examined in the impedance domain (the impedance being defined as the pressure rise over the square of the volume flow), which is done on Figure 8. As can be observed, the 9000 rpm fan is operating nearly at its local best acoustic point, whereas the other two are very close to partial load. The LES results are quite fairly rendering this trend at the suction side. Besides, another interesting phenomenon can be observed: the shape of the characteristics in the overload region is steadily changing as the design rotation speed is increased. For low design rotation speed, the overload region is louder than the best efficiency point (the noise is decreasing for increasing impedances), whereas the contrary can be observed for higher design rotation speeds (the noise is increasing for increasing impedances). This phenomenon is even more spectacular is only the broadband noise is depicted, as can be seen in the next section (s. Fig. 11 and 12).

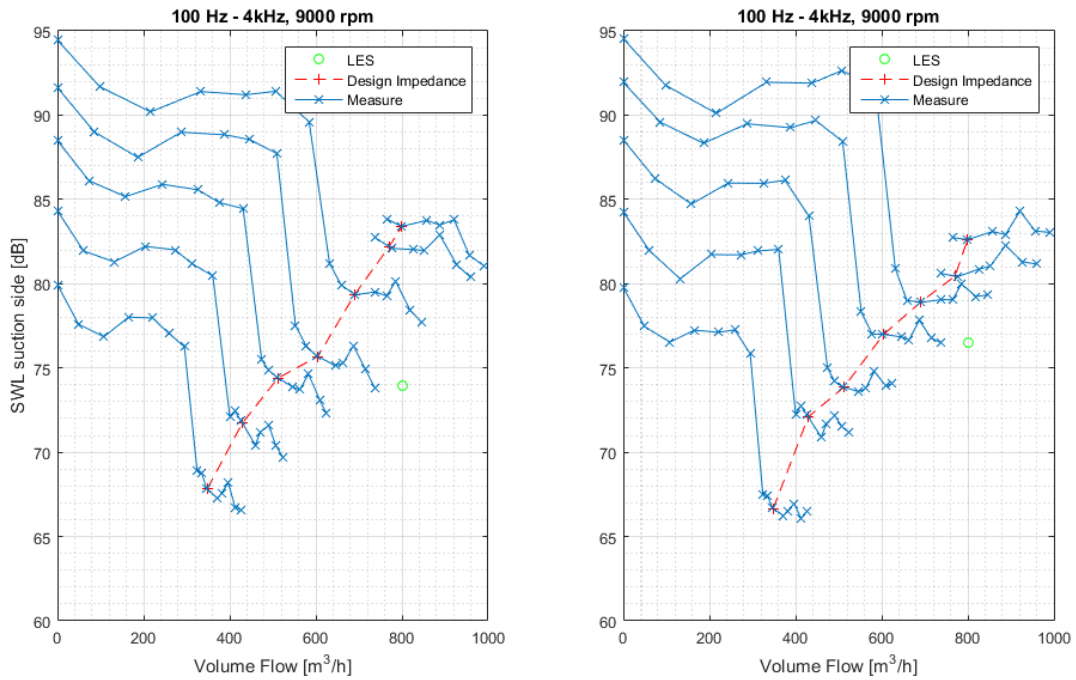


Figure 6: Sound Power characteristic field of the 9000 rpm design prototype, suction side (left) and pressure side (right).

Measurements at different speeds (blue) and along the design impedance (dashed red)).
 LES results are respectively represented in green.

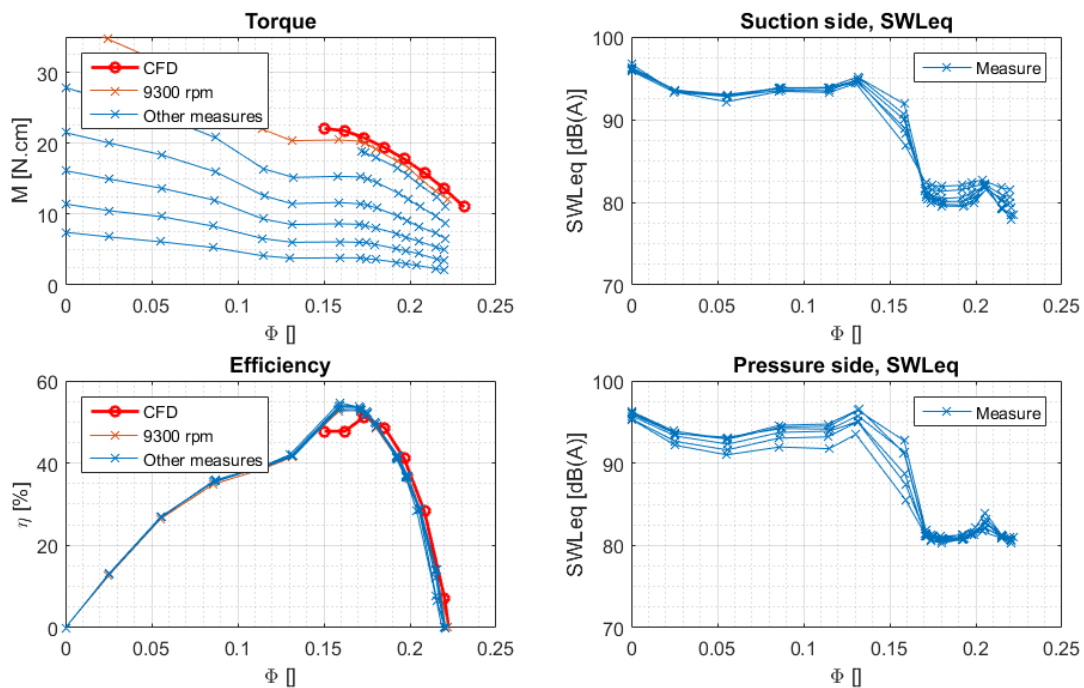


Figure 7: Results overview for design speed 9000 rpm:

Moment, aerodynamic total efficiency and rotation speed corrected Sound Power:
 5.5th power of rotation speed (top right: suction side) and 5th power of rotation speed (bottom right: pressure side)

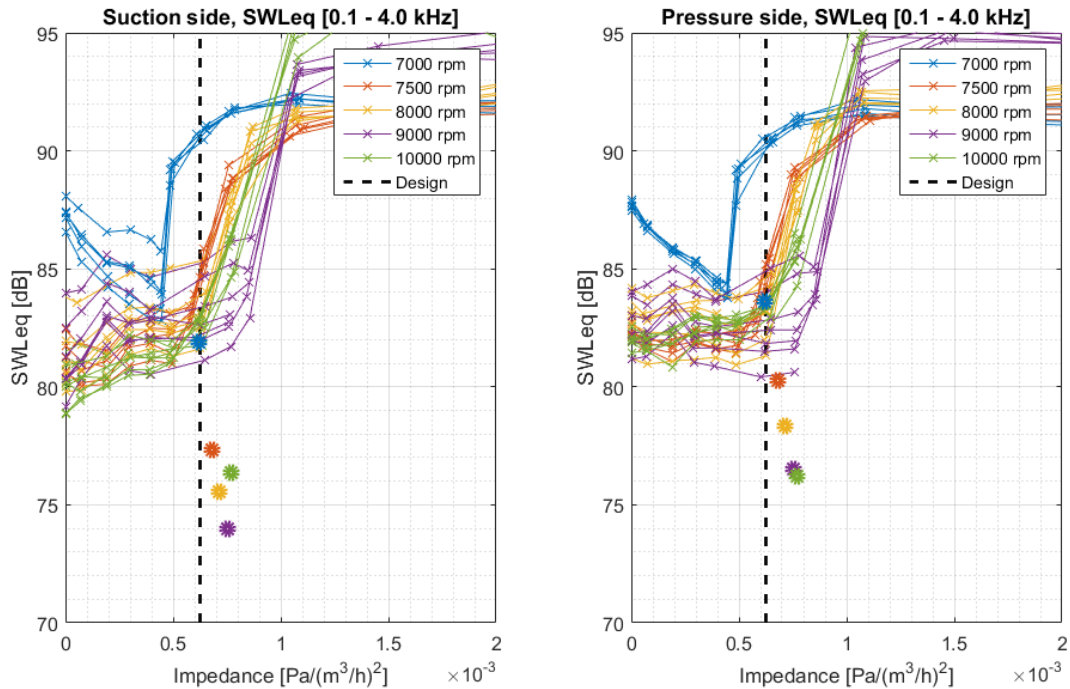


Figure 8: Comparison between LES/FWH based acoustic predictions and measurements: normalized SWL computed over the 100 Hz – 4000 Hz range and represented along the impedance. LES predictions are represented with stars. The normalization rotation speed is the design rotation speed.

BROADBAND NOISE CONTRIBUTION

In order to better analyze the measurements, a 9 points median filter has been applied to every PSD, cutting all harmonics of the rotation speed order and therefore highlighting the aeroacoustic broadband noise contribution: imbalance, motor orders and blade passing frequencies have therewith been successfully filtered out. An illustration of the method is given on the Figure 9.

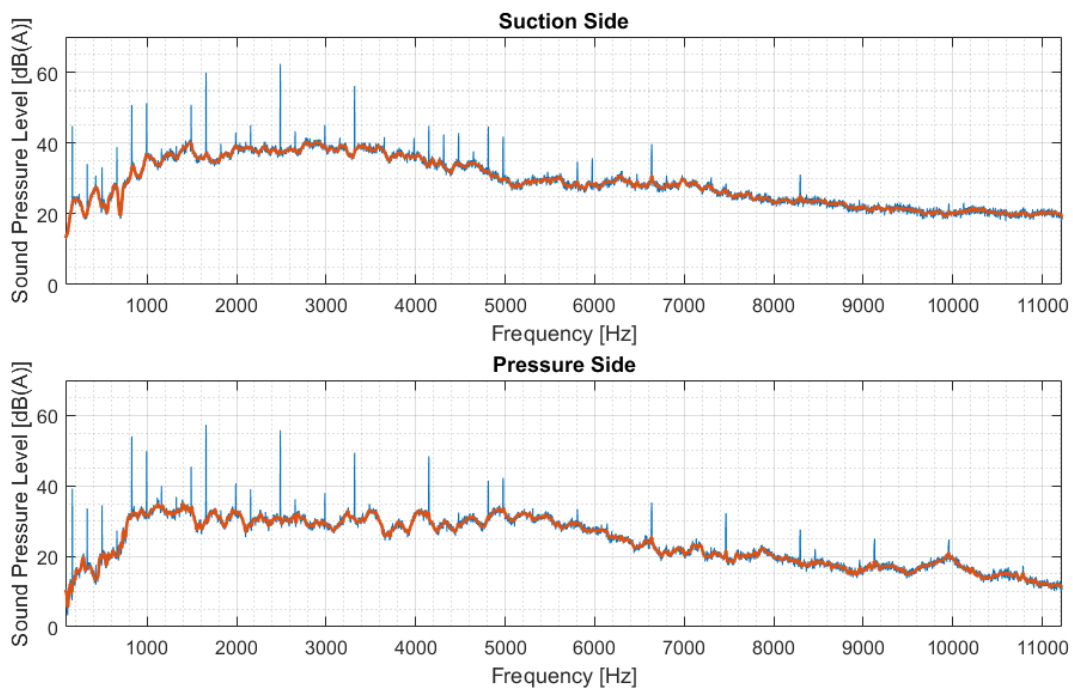


Figure 9: Example of median filtering applied on a PSD.

A deeper analysis of the aforementioned abnormal noise showed that a flow detachment takes place in special conditions. Indeed, a good overlap of the curves is obtained if a Strouhal number is used. The 9000 rpm case is represented on the Figure 10. In the present case the Strouhal has been based on absolute inflow velocity and the blade depth (blade chord projection along the rotation axis). All curves affected by the abnormal noise present a hump at Strouhal number of 0.55. The hump amplitude is maximal for 9000 rpm, which is a hint that an aeroacoustic coupling may take place. Two further humps are visible at Strouhal numbers 0.05 and 0.2. These humps are visible in a large operating volume flow range extending over the saddle point. Given the rather large tip clearances, one of these humps may be related to tip vortices.

An overview of the overall and broadband SWL characteristics is respectively given on the Figure 11 and 12. The LES based SWL predictions are represented for illustration purposes too, even if computed differently (integrated between 0.1 and 4.0 kHz, and not dB(A) weighted). The normalization rotational speeds are taken from the Table 2, so that all fans are reaching the design point at the design impedance. The phenomena observed on the Figure 8 are here clearer. The 9000 rpm fan does present a local best acoustic impedance greater than the other fans. These results are observed on both sides of the fan. Even if the comparison with predictions is not perfect, the same conclusion can be formulated: there exists an optimal rotation speed for the design point at which broadband noise is minimal. Another interesting conclusion can be taken when comparing the Figures 11 and 12: from all design rotation speeds, the 9000 rpm curves are the most affected when only the broadband noise contribution is selected. This means that the 9000 rpm design is the most tonal. Finally, it can be noticed that the SWL normalization better works when only the broadband noise contribution is observed. This may indicate that the broadband noise contributions are mostly generated on the blade boundary layers (self-noise, for instance), as 5th power is often a sign of non-compact dipole noise.

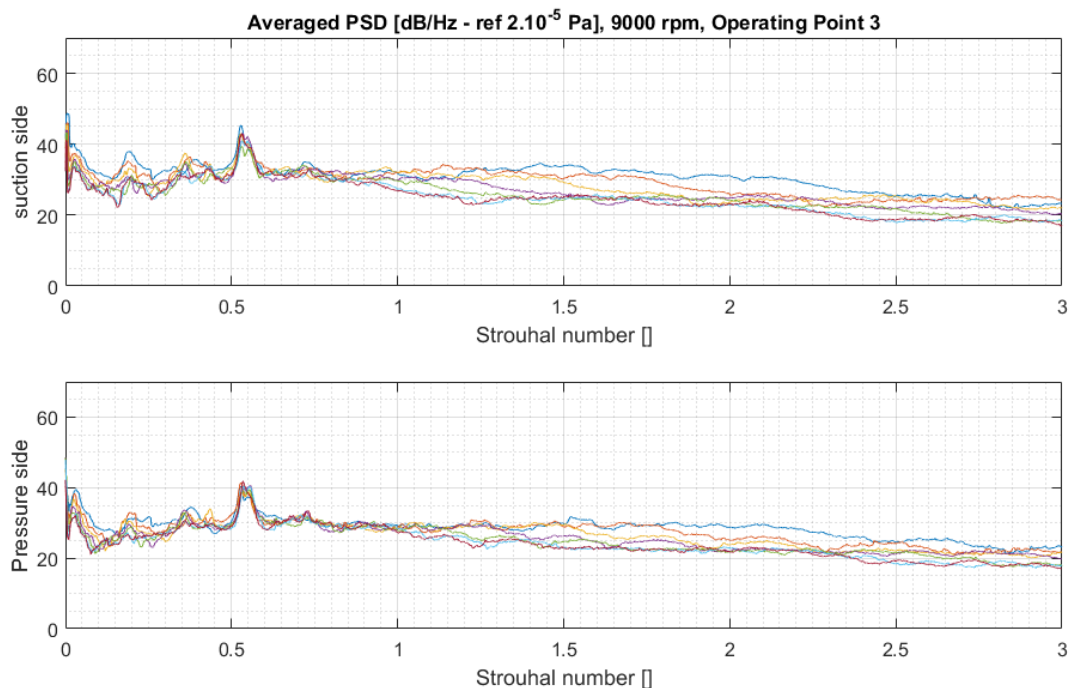


Figure 10: Non-dimensional, over the microphone averaged PSD. Operating point 3 from characteristic 9000 rpm. The PSD are normalized with the 5th power of the rotation speed.

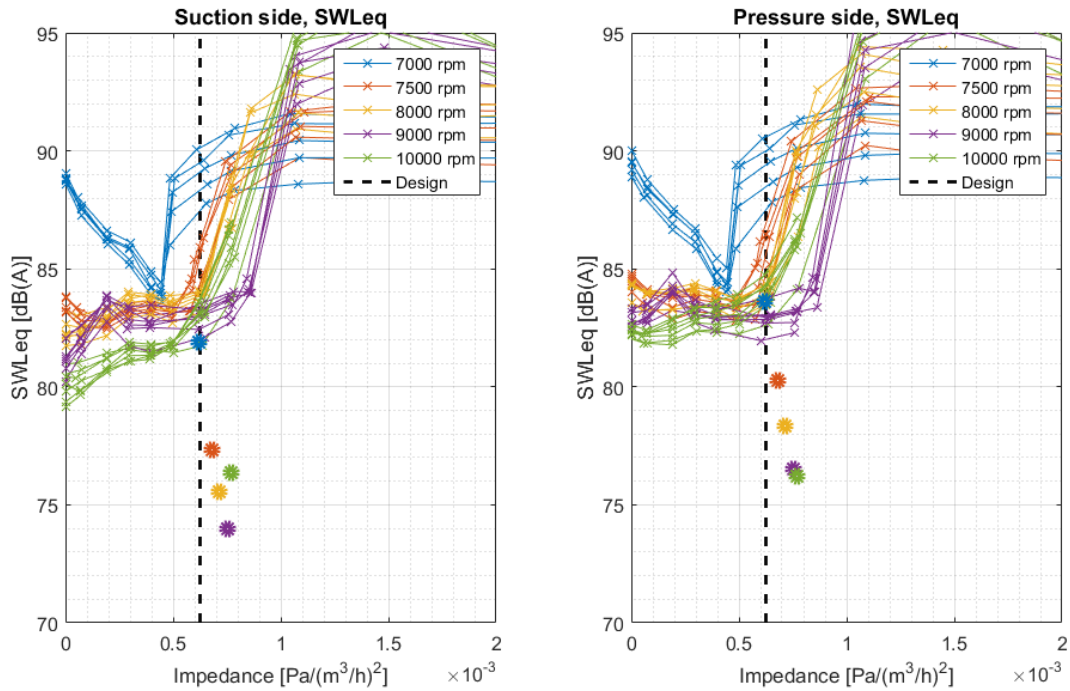


Figure 11: Overview of the overall radiated noise. The averaged SWL are compensated with the 5th power of the rotation speed required to achieve the design point (s. Table 2).

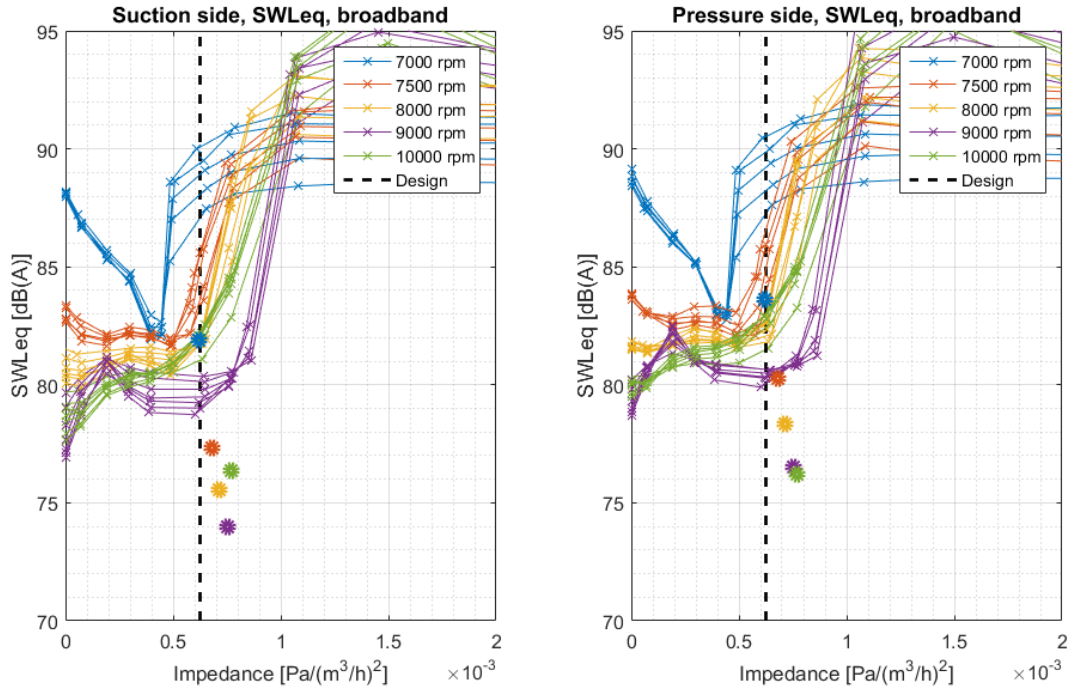


Figure 12: Overview of the broadband radiated noise. The averaged SWL are compensated with the 5th power of the rotation speed required to achieve the design point (s. Table 2).

CONCLUSIONS

The present communication investigated the relationship between design rotation speed and broadband noise. Experimental results following RANS and LES/FWH based predictions were presented. Non expected phenomena were explained. The comparison between numerical predictions and results is not optimal and discrepancies could be observed on the pressure rise characteristics as well as the radiated noise. The main reason to this is believed to be the larger tip clearances exhibited by the experimental prototypes. Nevertheless, similar trends could be observed.

The present communication confirmed that the rotation speed is a design parameter, which has a strong influence on the noise characteristics of a fan. In the present design strategy (resulting in variable fan depth), it has been shown that an optimal design rotation speed could be found. The optimal fan not only exhibits the furthest saddle point from the design point, it also has the most tonal acoustic spectrum, as could be shown by separately analyzing the broadband noise characteristics.

BIBLIOGRAPHY

- [1] A. Moreau, S. Guérin – *The Impact of Low-Speed Fan Design on Noise: An Exploratory Study*, Trans. ASME, J. Turbomach., Vol. 138, pp. 081006-1–081006-13, **2016**.
- [2] Y. Rozenberg, M. Roger – *Effect of Blade Design at Equal Loading on Broadband Noise*, AIAA J., **2006**.
- [3] P. Buchwald, D. M. Vogt, J. Grilliat, W. Laufer, M. B. Schmitz, A. Lucius, M. Schneider, *Aeroacoustic Analysis of Low-Speed Axial Fans With Different Rotational Speeds in the Design Point*, J. Eng. Gas Turbines Power 140(5), **2017**.